Review

Intravital Imaging with Two-Photon Microscopy: A Look into the Kidney

Vincenzo Costanzo [1] **and Michele Costanzo** [2,3,*]

1 Department of Experimental, Diagnostic and Specialty Medicine, University of Bologna Alma Mater Studiorum, 40126 Bologna, Italy; vincenzo.costanzo3@unibo.it
2 Department of Molecular Medicine and Medical Biotechnology, University of Naples Federico II, 80131 Naples, Italy
3 CEINGE–Biotecnologie Avanzate S.C.R.L., 80145 Naples, Italy
* Correspondence: michele.costanzo@unina.it

Abstract: Fluorescence microscopy has represented a crucial technique to explore the cellular and molecular mechanisms in the field of biomedicine. However, the conventional one-photon microscopy exhibits many limitations when living samples are imaged. The new technologies, including two-photon microscopy (2PM), have considerably improved the in vivo study of pathophysiological processes, allowing the investigators to overcome the limits displayed by previous techniques. 2PM enables the real-time intravital imaging of the biological functions in different organs at cellular and subcellular resolution thanks to its improved laser penetration and less phototoxicity. The development of more sensitive detectors and long-wavelength fluorescent dyes as well as the implementation of semi-automatic software for data analysis allowed to gain insights in essential physiological functions, expanding the frontiers of cellular and molecular imaging. The future applications of 2PM are promising to push the intravital microscopy beyond the existing limits. In this review, we provide an overview of the current state-of-the-art methods of intravital microscopy, focusing on the most recent applications of 2PM in kidney physiology.

Keywords: intravital imaging; two-photon microscopy; kidney disease; renal physiology; machine learning

1. Introduction

Fluorescence microscopy represents one of the most used approaches in the biomedical field to elucidate the cellular processes in vitro [1–3]. Cells or isolated tissues are cheap and easy-to-use systems that allow to gain crucial insight on cellular and molecular mechanisms using classical or high throughput technologies [4–6], and test the ability of pharmacological molecules to treat genetic diseases [7,8]. Nevertheless, these methodologies show some limitations if one takes into account that cells are very dynamic in changing their characteristics when isolated from the native environment and, consequently, cannot reproduce the complex physiological organization of living organisms. Accordingly, the in vivo systems may be considered more appropriately and suitably adoptable for studying diseases, owing to their ability to mimic human disorders and the consequent higher reproducibility of the results.

Confocal microscopy is a milestone in the field of microscopy. This type of microscopy uses one-photon fluorescence excitation, which enables more detailed images if compared to the conventional fluorescence microscopy [9]. The enhanced performance of confocal microscopy is made possible by the presence of the pinhole (and its particular conformations) able to reject the unnecessary light providing improved resolution [10]. The applications offered by confocal microscopy have been widely described over the years and they include the tracking of single organelles [11], the real-time monitoring of cell division mechanism [11], the study of gene expression [12], and the evaluation of cell trafficking [13]. The ability to optically section a specimen, obtaining 3D reconstructions,

is an additional real possibility offered by confocal microscopy. Especially, such prospect is crucial to perform quantitative analysis and volumetric measurements of dynamic cell processes. Although it has been largely adopted to provide insights into several cellular mechanisms, the use of confocal microscopy remains limited when a living sample or a thick specimen is imaged, owing to the presence of the high light scattering and the significant effect of the photobleaching.

To overcome such issues, currently, the two-photon microscopy (2PM) is thought of as the gold standard method for intravital imaging in living animals. Thus, the 2PM grants the acquisition of 3D movies and real-time high-resolution images of living cells and tissues, allowing a great advancement in the study of organ regulatory mechanisms [14].

This review discusses the basic principles of 2PM and the main advantages offered by this brilliant imaging approach. The most recent and fascinating applications of 2PM, with a particular focus on kidney physiology, are discussed. In addition, the use of analysis software and machine learning algorithms for the elaboration of images and videos are also explored.

2. Principles of Two-Photon Microscopy

2PM offers stunning images and real-time movies of the cellular and subcellular physiology in living animals. This technique has been widely used by researchers in the last decades to address important biological questions, taking advantage of its deeper laser penetration and low phototoxicity. In comparison to the previous technologies, such as confocal microscopy, 2PM uses a long-wavelength laser in the near infrared range (700–1000 nm) and exploits the simultaneous arrival of two low-energy photons of light on the sample [15,16].

With the conventional one-photon excitation, one photon is driven to a fluorophore, which subsequently moves from the ground state to a higher-energy state. Thereafter, it loses the acquired energy back to the ground state, thus emitting a photon of light. By contrast, the two-photon excitation relies on the simultaneous absorption of two photons, which show half the energy of the single-photon excitation event. Being inversely proportional to the energy of a photon, the wavelength of the two photons is approximately doubled with respect to the one used by one-photon excitation to reach the energy state transition. Thus, the singlet excitation state of the two photons is equivalent to that obtained by one-photon absorption, producing an identical emission fluorescence between the two optic phenomena [17]. This scheme of photon absorption/emission is explained by the Jablonski diagram, as reported in Figure 1.

The probability that the two photons hit a fluorophore at the exact moment ($\sim 10^{-18}$ s) is made significant by increasing the photon flux ($> \sim 10^6$ times) in a short time window with respect to the one-photon system. Efficient concentration of the photon flux in time can be accomplished by using a higher-energy laser with a tighter focusing, such as the ultra-short pulsed laser source, that permits to increase the density of the photons, concentrating them into discrete pulses. Such laser source permits to increase the peak power of the pulses relative to the time-averaged power. Additionally, a spatial concentration of the photon flux is achievable using high-numerical aperture objectives which, focusing this flux also in space, increase the probability of the simultaneous incidence of the two photons [17].

The concept of two-photon fluorescence was first theoretically suggested by the physicist Maria Göppert-Mayer in the 1930s [18], but experimentally put into practice approximately 30 years later by Kaiser and Garrett who investigated the generation of blue fluorescent light by exciting the europium doped calcium fluoride (CaF_2:Eu^{2+}) with red light [19].

The efficiency of an optical system is defined by its resolution, as the capability to distinguish two close signals as separate objects, determining the minimum distance between them [20]. This spatial resolution, which includes the axial and the lateral resolution, may be affected by changes in many parameters, such as the wavelength of the laser source, the magnification and the numerical aperture of the used objectives, and the aperture size of

the pinhole. In particular, higher numerical aperture, larger field of view, and lower light scattering improve the spatial resolution [17]. Since the 2PM uses doubled wavelength, the resulting resolution would be approximately half if compared to that ofconfocal microscopes. In a confocal system, the spatial resolution of the acquisitions is boosted by adjusting the pinhole ahead of the detector, thus discarding the out-of-focus fluorescence. Truly, this difference in resolution between the two approaches becomes minimal if one considers that a quota of resolution is progressively lost in the confocal microscope when the pinhole is even minimally opened [21]. Consequently, the 2PM shows only a slightly reduced spatial resolution compared to the one-photon excitation systems [22]. However, being dependent on the number of photons collected, the spatial resolution is inversely proportional to the temporal resolution, and its increase reduces the acquisition time needed for the measurements [23]. The temporal resolution of an imaging system is characterized by many determinants, such as the quantum yield and other molecular factors. As explained by Mondal, the temporal resolution can be quantified by considering the time necessary by the excited molecules to complete a single excitation-emission transition. Consequently, the time required for almost all molecules (~99.9%) to relax back from the excited state to the ground state denotes the limit of temporal resolution, further defined by the recycle time of the fluorescent molecule [24].
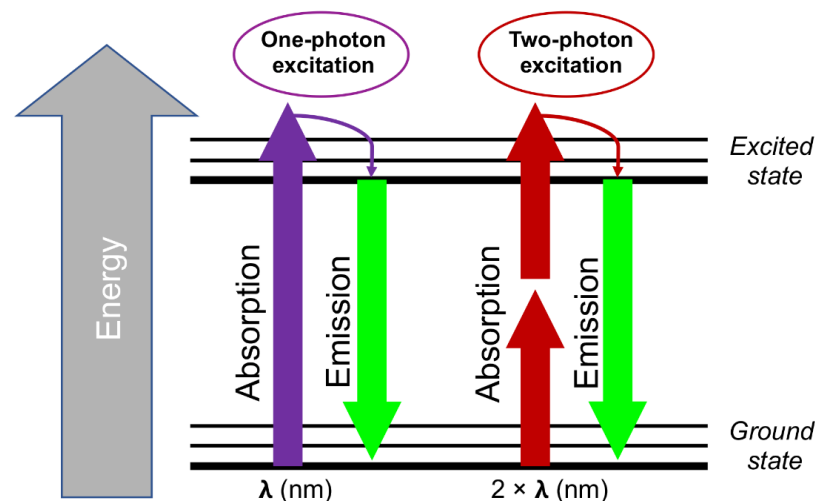

Figure 1. Jablonski diagram for one-photon and two-photon excitation fluorescence. The absorption by a fluorophore of a single photon with sufficient energy allows the one-photon excitation (purple arrow) of the molecule. The two-photon excitation occurs upon the simultaneous absorption of two half-energy photons (red arrows). The resulting emission fluorescence (green arrows) is identical for both the optical phenomena. For one-photon absorption, λ is the excitation wavelength, whereas that necessary for the two-photon system is approximately double ($2 \times \lambda$).

The latest state-of-the-art optic systems employ super-resolution microscopes (SRM) that are able to significantly enhance the spatio-temporal resolution [25]. Accordingly, SRM may perform at increased resolutions over the usual resolution limit, popularly recognized as the Abbe diffraction limit, enabling to image detailed structures as small as tens of nanometers, such as the cell organelles. Some of the techniques developed for the SRM are photoactivated localization microscopy (PALM), fluorescence PALM (fPALM), stimulated emission depletion microscopy (STED), stochastic optical reconstruction microscopy (STORM), ground state depletion microscopy (GSDIM), and structured illumination microscopy (SIM). The majority of these (PALM, fPALM, STORM, GSDIM) enable a super spatial resolution at the cost of lower temporal resolution. By contrast, other techniques including multiphoton multifocal microscopy, multifocal plane microscopy, multiple excitation spot optical microscopy, and multiple light-sheet microscopy (LSM) advantage the increase of the temporal resolution [24]. Notwithstanding, LSM uses a thin sheet of light to

illuminate the plane of interest with a resulting improvement in terms of light efficiency and high volumetric imaging speed. LSM provides great benefits for the biological research since it can be easily applied to large samples with low phototoxicity and very high contrast of images. Despite this, the imaging of thick specimens produces high light scattering resulting in aberrations, contrarily to 2PM. In addition, LSM sacrifices the spatial resolution for the temporal one to permit fast acquisitions for prolonged imaging period. Owing to such limitations, LSM has been coupled to 2PM. This combined system represents an advancement in tissue imaging and permits both to increase the resolution and decrease the light scattering, especially in thick specimens [26]. Fundamentally, 2PM has an optic resolution limited to around 250 nm [27]. This diffraction limit can be bypassed coupling 2PM with SRM. An innovative integrating approach, called two-photon scanning patterned illumination microscopy (2P-SPIM), has been developed by Urban and colleagues who obtained a lateral resolution of 141 nm, representing an improvement of approximately 1.9-fold over the 2PM system alone [28].

Nonetheless, the employment of 2PM allows to obtain additional several advantages. First, there is less phototoxicity due to the low energy of the two photons, allowing continuous observations of the samples over the time [17]. This is particularly beneficial when thick samples or living organs are imaged. In addition, the laser penetration in the tissue is deeper in consequence of the reduced light scattering, permitting to image up to 150–200 μm in the kidney, while in the brain or other less heterogeneous organs more than 1 mm of deepness can be reached [29,30]. However, this depth is about 3 times higher than confocal microscopy [31], as schematically shown in Figure 2. Moreover, the out-of-focus signal of the image is reduced and the fluorescence intensity is high only in the focal plane, reducing the photobleaching and avoiding the necessity of a pinhole [32,33]. Owing to all the above-mentioned advantages, 2PM is able to capture dynamic events in living animals, incorporating the complexity of hormonal factors with subcellular resolution, becoming the gold standard approach for intravital imaging in animal models.
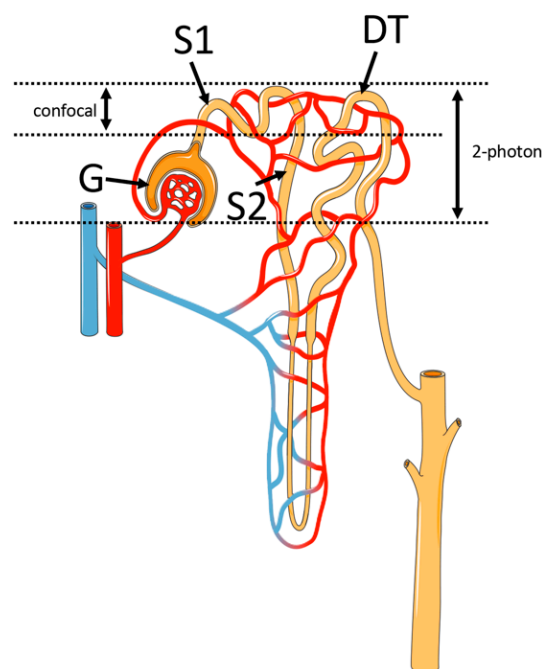

Figure 2. Schematic representation of the renal structures identified with 2PM. The nephron segments that are visible with confocal and 2PM are shown. As indicated by the vertical arrows, 2PM allows the renal structures to be imaged about 3 times deeper compared to confocal microscopy. G = glomerulus; S1 = S1 proximal convoluted tubule; S2 = S2 proximal convoluted tubule; DT = distal tubule. This figure was drawn adapting the vector image from the Servier Medical Art bank (http://smart.servier.com/; last accessed on 22 February 2022).

3. Main Applications of Two-Photon Microscopy

3.1. Renal Autofluorescence to Study Metabolic Functions

The renal metabolic functions may be studied indirectly by easily analyzing the urine samples collected as easily accessible liquid biopsy from individuals. The specific urinary patterns of molecules detected is an indirect measure of the pathophysiological status of patients [34–36].

Instead, the application of 2PM provides unique and direct opportunities to perform morphological and functional studies, even without external labeling or exogenous dyes, taking advantage of the endogenous autofluorescence properties displayed by several molecules. For example, the lysosomal and mitochondrial NADH fluorescence naturally exhibited by the renal tubules enables the visualization of some kidney structures [37]. This intense autofluorescence allows to recognize the proximal tubules that are very rich in mitochondria and lysosomes, while other nephron segments poor in such organelles, such as the distal tubules, and the collecting ducts appear as dark empty patches [38]. The superficial glomeruli, lacking of any fluorescence, appear likewise as large dark empty spaces close to proximal tubules, as visibly appreciable in Munich Wistar Frömter (MWF) rats. Thus, the autofluorescence can be very supportive in recognizing and defining the renal components without using exogenous dyes.

This approach has been important to clarify the metabolic profile in S1 and S2 proximal tubules at the physiological level. Indeed, Bugarski et al. demonstrated that the mitochondrial NAD(P)H expression is comparable between the two populations of tubules. However, S2 proximal tubules displayed a more intense signal at the cytosolic level and this seems to be justified by their main function to maintain the pool of cellular glutathione. Moreover, a higher expression of flavoproteins is also displayed in S2 than S1, reflecting a different regulation of glutamine and nitrogen metabolism [39,40]. In addition, it was shown that S2 proximal tubules are more dependent on glucose metabolism than S1 tubules as confirmed by the drastic signal reduction in this nephron segment upon the stimulation with a glucose inhibitor [39]. This is in agreement with previous studies showing a damage of rat S2 isolated tubules when a glucose inhibitor was used [41].

As shown by Hall et al., NADH also provides a crucial read out of the metabolic state of renal tubules after renal injury, such as ischemia reperfusion injury (IRI). In particular, the authors demonstrated that following IRI, the membrane potential quickly dissipates leading in turn to the fragmentation and shortening of the mitochondria in proximal tubules, while the distal tubules better maintained the membrane potential [42]. This may be crucial to investigate the electron transport chain function, which provides information regarding the redox state of the mitochondria [43]. These data pave the way toward the therapeutic application of this technical approach to monitor the eventual improvement of the membrane potential and the overall metabolic function, following the administration of IRI-targeting drugs.

Notwithstanding, the main drawback in using the renal autofluorescence to investigate the metabolic functions is evidenced when external probes are used concurrently. In fact, in these cases, the tissue autofluorescence may overlap with the emission signals of the external probes, rendering the data obtained from the analysis doubtful [44].

3.2. Second Harmonic Generation (SHG) to Study Renal Fibrosis

Additional applications of 2PM make use of the second harmonic generation (SHG) technology, often called frequency doubling, which is a non-linear optic phenomenon that takes advantage not of absorption but of the Rayleigh scattering. In particular, two photons with the same frequency interact with a non-linear material and are finally 'combined' resulting in frequency-doubled photons [45–47]. Consequently, SHG signals are revealed at the half of excitation wavelength, and can be detected simultaneously with the renal autofluorescence, providing the overall imaging perspective of the organ. The advantages obtained by this imaging approach are understandable. SHG is particularly beneficial

as it does not require external fluorescence labeling, hence circumventing the effects of photobleaching and the issues related to molecules administration.

One main application of SHG relies on the possibility to visualize collagen fibers [48], as well as muscles myosin [49] and microtubules [50], showing high specificity when the signal is detected. Indeed, SHG allows to distinguish type I and type III collagen fibers, whereas non-fibrillar material, such as type IV collagen, cannot be revealed in tissues. Additionally, no tissue preparation is required: fresh, fixed, and frozen preparations as well as living organs can be analyzed, ensuring the reproducibility of the technique and minimizing the variability shown by conventional histological techniques. Furthermore, 3D reconstruction of imaged SHG is possible in living samples thanks to the high penetration power of the multiphoton laser. In turn, this permits to perform volumetric analysis of the tissue of interest. Accordingly, the application of SHG in the field of nephrology is well documented and many research groups have used SHG to image and quantify the fibrosis progression in renal diseases, showing the high potentiality as a pejorative predictor of nephropathies in many renal injuries [48,51,52] and in translational cancer research [53].

3.3. Single-Nephron Glomerular Filtration Rate (SNGFR) Assessment

A reliable measure of kidney function is provided by the glomerular filtration rate (GFR), which is one of the most important renal parameters taken into account by clinicians for diagnosing renal disorders or monitoring chronic renal diseases [54]. The kidney functionality with the measurement of the GFR, as well as the kidney volume and the renal clearance may be complemented by assessment with other imaging techniques such as dynamic micro-PET (Positron Emission Tomography) analysis after injection of radiotracers [55].

The GFR indicates the overall filtration function of the kidney, whereas the single-nephron GFR (SNGFR) considers the individual filtration events, assessing the function of individual nephrons. Since its discovery, the evaluation of SNGFR has been established as one of the key parameters to evaluate the renal function [56]. In fact, in some pathological conditions, such as the diabetic nephropathy, the total GFR may remain unchanged, even after a significative nephron loss (50%), because of the compensatory hyperfiltration of single nephrons [56]. For these reasons, evaluating the SNGFR provides more accurate and precise information regarding the glomerulus dynamics, as well as the determination of the mechanisms of tubular reabsorption and secretion.

Historically, the micropuncture was the first technique employed to elucidate the mechanisms of renal function and has been extensively used for many years as the gold standard technique for the SNGFR calculation in vivo. However, this technique is laborious and demanding in virtue of the very complex surgical preparation of the animals and the sophisticated equipment required [57]. For these reasons, the assessment of SNGFR represents one of the most attractive applications of 2PM in kidney physiology. Accordingly, Kang et al. developed and implemented a 2PM-based method, consisting in the observation and quantification of the fluorescent decay time of a low-molecular-weight dye between two regions of interest selected within a tubule [58]. In particular, they used multiphoton resonant scanners, which are optional galvanometric mirrors able to perform higher full-frame acquisitions (>20 Hz) than basic 2PM. This approach provided reliable data comparable to the old-fashioned micropuncture. Notwithstanding, the implementation of 2PM with resonant scanners requires additional costs for the users. Furthermore, the high-speed acquisition offered by this imaging modality may increase the noise of the detected signal, hence forcing the investigators to use imaging software to analyze the data and improve their quality.

Instead, an innovative method that does not employ the resonant scanners was recently used to assess the SNGFR through the application of the linescan tool [59]. Linescan is a well-established 2PM method mainly exploited in kidney physiology to assess the erythrocytes velocity in renal vessels [60]. Linescan permits to acquire a region of interest (ROI) repetitive times reaching a very high temporal resolution, since the acquisition is focused only on a drawn line, instead of the entire field of view. This novel application, therefore,

does not require the implementation of expensive resonant scanners and can obtain even faster measurements (>400 Hz) than previous multiphoton approaches. Standing as a faster method, it permits to measure a higher number of tubules in the same animal during the experiment. This, in turn, would allow the investigation of new complex biological questions, such as the nephron heterogeneity. The linescan tool has been validated in models of increased (i.e., following low-dose dopamine administration) and reduced (i.e., following IRI) SNGFR, showing results comparable with conventional micropuncture and previous full-frame acquisition [59]. Notably, while conventional micropuncture only allows to measure a few tubules per single animal for SNGFR experiments, the linescan tool allows to analyze on average 15 tubules, hence improving the reliability of the study. The novel linescan-based approach is a reliable tool for the in vivo assessment of SNGFR in health and disease, thus representing a promising method for future preclinical investigations.

3.4. Organic Cations Transport Evaluation

Further applications of 2PM technology include the evaluation of the organic cations (OC) transport throughout the kidney. The excretion of OC mainly occurs along the proximal tubules by a secretion mechanism [61]. For the regulation of such mechanisms in humans, the organic cation transporter 2 (OCT2) is involved in the basolateral uptake of many OC in tubular epithelial cells, whereas the multidrug and toxin extrusion 1 and 2 proteins (MATE1, MATE2-K) mediate the apical secretion of OC. In rodents, the tubular secretion is mediated by the basolateral OCT1 and OCT2 transporters, and by the apical MATE1 [62]. Because of this fine regulation, the toxic substances (including antibiotics and diuretics) and the endogenous metabolites (such as catecholamines) are efficiently removed from the blood. Among these molecules, the uremic toxins are particularly dangerous since their accumulation can lead to chronic kidney disease [63]. Therefore, the development of methods to in-depth investigate the OC transport is required for the formulation of drugs and optimization of dosages.

The fluorescent organic cation 4-(4-(dimethylamino)styryl)-N-methylpyridinium (Asp+) has been proposed as a valid dye to study the OC transport in the kidney. The work of Hörbelt et al. [64] demonstrated for the first time that the secretion of OC can be elucidated in vivo in the rat kidney by means of the 2PM and Asp+ marker. Accordingly, the authors monitored the continuous distribution of the fluorescent signal in the renal tubules upon the endovenous administration of Asp+.

A very recent study exploited the potential of 2PM to extend the knowledge of renal OC transport by using the Asp+ dye [65]. The first attempt of the authors was to reproduce the results obtained by Hörbelt. The presence of the signal in the tubular lumen and the strong fluorescence along the apical membrane of proximal tubules detected during the in vivo experiments induced the investigators to test the hypothesis of a binding between Asp+ and albumin. Therefore, a combination of in vivo 2PM and PET approaches was used to investigate the binding of ASP+ with serum albumin. The data obtained by this work clarified that Asp+ may not be a convenient probe for the in vivo evaluation of OC transport, since the detected signal is likely affected by the presence of albumin. These in vivo observations have been demonstrated through in vitro assays, showing an enhancement of the Asp+ signal in presence of bovine serum albumin (BSA) and a blue shift of the emission peak. Finally, further confirmation comes by considering that the high Asp+ signal was detected in old rats, which likely show high levels of albumin in the ultrafiltrate, while this marker was not detectable in the lumen of young rats [64].

3.5. Renal Tissue Regeneration

Mammalian cells have limited lifespan; therefore, they need to be continuously replaced to ensure the morphological and functional integrity of an organism. Compared to other organs, such as liver and skin, whose cells are constantly renewed, renal tissue holds a lower cell turnover, thus showing limited regenerative ability. However, the replenish-

ment of renal cells is necessary to preserve the kidney function, despite the mechanisms of tissue regeneration still not being clear [66].

The conventional experimental approaches are not able to follow the renal regenerative process over the time, leaving a gap of knowledge in this field. The advent of 2PM has allowed to constantly monitor in real-time the dynamic reparative process in the kidney with unprecedent results. In particular, Schiessl et al. demonstrated with 2PM analysis, after applying an abdominal window on the mouse, that the interstitial cells are involved in the regeneration of the renal epithelium by a PDGFβ-mediated process [67].

Along the same lines, Zhang and colleagues recently exploited the 2PM and the abdominal window to investigate the regenerative therapies following acute kidney injury (AKI) [68]. In detail, the authors tested the ability of mesenchymal stem cells (MSC)-derived microvesicles (MVs) to regenerate the renal tissue in a transgenic mouse model of AKI. The data obtained showed that the injected MVs were able to travel to the injured kidney and promote the formation of efficient renal tubules through a Sox9-mediated mechanism. The therapeutic effect of MSC-derived MVs was further demonstrated by the evaluation of renal function. Indeed, the progression of renal fibrosis as well as the increase of blood urea nitrogen and serum creatinine typically detected after AKI were significantly reduced following the MVs administration [68]. These results show that 2PM and the abdominal window constitute a powerful combination to track in real time the distribution of single MVs in renal tissue and the repair process after a renal injury. This approach is promising for future studies aiming to explore the regeneration of other abdominal organs.

4. Imaging Data Processing and Machine Learning

The great potential of 2PM technology is counteracted by several drawbacks that make the experiments quite intricate, especially for the data analysis of acquired images. The movements of the animals under analysis due to the breathing may generate drifts and artefacts that complicate the experimental acquisition and the following data analysis. Particularly for the above-mentioned linescan procedure, a high stability in the field of view is required to ensure reliable results. This can be in part mitigated during the animal preparation with proper anesthesia and surgery. Noteworthy is the work of Rhodes [69], who discussed different methods of anesthesia, surgical approaches for intravital microscopy, and post-operative recovery procedures.

Some expedients may improve the image stability during the acquisition process. In particular, better results can be achieved by increasing the spatial resolution, i.e., to a full-frame 512×512 pixels that usually permits acquisitions with a temporal resolution of 1 frame-per-second. Such resolution, despite not being the highest reachable, may represent a compromise to concurrently avoid excessive animal movements and image moderately fast processes, such as glomerular permeability and protein/metabolite uptake [70]. On the other hand, faster cellular events (i.e., erythrocytes velocity) need to be tracked with higher temporal resolution, achievable by scanning smaller regions, for example using the linescan tool.

Also taking care of such precautions, many artefacts caused by animal movement can persist. A practical solution adopted when a video is taken relies in the motion compensation in the post-processing phase. As widely reported, several algorithms can be applied to improve the stability of time-series or z-stacks, through an alignment of the acquired frames one with the other or with reference frames [71]. For example, the "registration" plugin on the imaging software Fiji is particularly useful to stabilize the acquired movies, by the realignment of the x, y, and z positions within a ROI [72]. In addition, many other corrections can be performed with the same software image. After the image acquisition, some filters can be applied to enhance the contrast, change the brightness, and smooth the edges [73].

Even often, imaging data processing following acquisition with 2PM may be hampered by blurred and noised images. A certain amount of light arriving on the sample inevitably leads to produce a noised signal especially when the photons reach the dark regions.

However, the signal-to-noise ratio (SNR) cannot be raised by simply changing the spatial resolution, since it would alter the interpretation of the examined events. In fact, one of the main tasks of the imaging processing tools is to suppress the image noise, referred to as the "denoising" process. Many tools and software have been developed in order to increase the SNR, thus improving the quality of the signals. On the other hand, as consequence, denoising methods may generate artefacts, flatten the edges, or exclude significant details within the images [74]. To overcome these issues, some algorithms may help reducing the noise in the pictures acquired by 2PM, preserving the samples even for quantification purposes [74].

Furthermore, the high penetration depth offered by 2PM progressively limits the quality of the images as a consequence of the light dispersion throughout thick tissues, resulting in a loss of contrast. The contrast, described as the ratio between the in-focus and out-of-focus signals, can be enhanced by rejecting the out-of-focus background in deep tissue imaging. Xiao and Mertz have improved a technique based on this principle of the background rejection for 2PM, named differential aberration imaging (DAI) [75]. This strategy removes the background through the comparison, and subsequent subtraction of one aberrated image from one unaberrated. Subtracting the aberrated image empowers the resulting contrast by retaining the in-focus signal. The authors specified the DAI approach as advantageous for 2PM, since neither further optical features nor extremely powerful computational systems are required [75].

Recently, a great development in the artificial intelligence (AI) techniques has been achieved thanks to their beneficial assistance to researchers worldwide. Machine learning (ML) is a subfield of AI developed to assist data and experimental observations, particularly exploited in the field of biomedical imaging [76]. Modern ML approaches have empowered the imaging data processing by providing automated and semi-automated algorithms to challenge with the complexity of the data generated by high throughput technologies. ML works by elaborating a computer program that is trained to learn to recognize and predict patterns [77]. In detail, ML algorithms generate mathematical models established by "training" and "ground truth" observations, by which they can accomplish classifications and predictions analysis [78]. While traditional ML models, e.g., random forest, classify and predict data on the basis of selected quality features, the deep-learning models, including the neuronal networks, represent another subtype of AI working to automatically extract features from the images [78].

These newest approaches, in fact, hold the potential to automatically detect, emphasize, segment, and classify different anatomical structures as well as injuries of interest in a faster and more reliable way with respect to the human visualization.

The AI offers the main advantage in saving time during the analysis of microscopy data. Indeed, a lot of crucial information could be extracted from a dataset of pictures in a shorter time than required by a manual approach. Moreover, the automatization of the analysis only needs an example of the image to be classified. Accordingly, neither specific parameters nor particular settings are necessary to drive the segmentation process. ML-assisted algorithms ensure reliable and accurate results following a robust training phase with respect to the manual analysis, which is predisposed to human error due to fatigue and distraction. Furthermore, the user can monitor at any moment the training process, modify the selected features, and control the segmentation efficiency, thus ensuring a finely optimized process. ML has shown surprising benefits for different medical applications, especially in the field of modern pathology and in the cancer field [79]. ML approaches have been shown to be particularly advantageous in assisting fluorescent microscopy studies. One of the most used ML applications is the thresholding of fluorescent images to obtain segmented images. This procedure may be complex with manual systems, especially when tightly packed tissue, such as cells within a tumor, are considered [80].

One recent example of a ML tool is represented by ilastik, an open source and semi-automated segmentation software [81]. This user-friendly tool provides the investigators with the main advantage of analyzing images and videos without particular programming

or computational skills. Users can adjust the workflow according to the biological question arisen by giving a specific training to obtain predictions masks. These latter are produced upon the selection of input given to the software as short brush. Different features, including shape, color, and texture, are used to segment the image of interest in specific classes. After performing an initial training phase, the algorithm is further able to perform a classification of many other images never seen before with similar features. This represents a much smarter and faster tool to segment images or video compared to conventional analysis approaches (for example, the imageJ software). Moreover, the ability of the software to automatically segment the images ensures the reliability and reproducibility of the results, overcoming the arbitrary analysis offered by previous tools.

5. Discussion

In the last decades, intravital 2PM has become the elite technique for studying the pathophysiology in animal models, especially for the kidney, due to the several advantages offered in comparison to confocal microscopy. The development of sensitive probes and powerful detectors enabled to gain stunning results as never before. In addition, the software for data analysis and the machine learning-based algorithms helped to analyze imaging data faster and with more reliability than before.

Here, we reviewed the most recent applications of 2PM, mostly focusing on the SNGFR assessment, the OC transport evaluation, and the renal tissue regeneration, which are among the most crucial points in kidney physiology. In particular, the evaluation of SNGFR values by the linescan tool represents a technical advancement that will be decisive to test pharmacological drugs able to revert pathological injuries or study other processes, such as acid-base alterations and diuretics administrations. The linescan method for 2PM in analyzing the SNGFR requires no resonant scanners because of the very high temporal resolution it is able to achieve. Moreover, more data points along each tubule can be obtained, providing the opportunity to study more precisely the tubular reabsorption of water and other molecules. What is more, this innovative method permits to improve the study of the renal function not only in rats but also in mice, the latter being almost prohibitive with the conventional micropuncture technique. Additionally, linescan-based 2PM permits to measure in the same animal a higher number of tubules for SNGFR assessment compared to the micropuncture, thus increasing the accuracy of the data and the statistical significance of the results. There is also a real possibility to perform repeated SNGFR measurements on the same tubules over several days/weeks if the linescan tool is combined with the existing approach of abdominal window. This represents an advancement compared to conventional micropuncture, allowing to perform new studies of nephron recovery after chronic kidney disease or other injury models.

Despite the exciting endless applications, the other side of the coin of the intravital imaging by intravital 2PM is represented by some limitations and drawbacks [82]. These include: (*i*) animal surgical preparation; (*ii*) limited laser penetration into the tissue; and (*iii*) quantitative analysis starting from image acquisitions. First of all, animal models are needed for in vivo imaging and a strong expertise is required for both animal preparation and microscopy management. As mentioned, proper anesthesia and surgical interventions are crucial to maintain the physiological breathing of the animals and minimize their movements. In particular for renal imaging, after adequate anesthesia, the animals are tracheotomized to facilitate the breathing, and the vein and artery are cannulated for the infusion of fluorescent probes and for monitoring the pressure, respectively. Then, a flank incision is made, and the left kidney is usually externalized. Subsequently, the animals are placed under the microscope with the exposed kidney positioned in a cell culture dish filled with warmed physiological saline solution [83]. Performing a 2PM experiment with a microscope objective positioned below the kidney generally provides more stable conditions and minimizes the movements due to breathing and the heart beating [16,32,33,70,83]. During such experimentations, the arterial pressure, the body temperature, and the breathing should be continuously kept under surveillance in order to

ensure the animal wellness and to monitor the normal kidney function. At the end of the experiments, the animals are euthanized, or they are surgically sutured and employed in further experiments [84].

Although empowered with respect to the confocal microscopy, the laser penetration of 2PM is limited at 150–200 μm in the kidney, restricting the imaging power only to the renal cortex. In fact, the majority of the glomeruli and the renal medulla are not visible with conventional fluorescence imaging techniques. Despite this, the visualization of the glomeruli can be partially enabled by 2PM using the MWF rats, which exhibit many glomeruli immediately located under the renal capsule [85]. As an alternative, recent works underline the possibility of using clearing techniques to study ex vivo the structures sited in the medulla [86,87]. Nonetheless, further strategies may permit a deeper imaging using enhanced laser power, longer excitation wavelength, or high numerical aperture of the objective lens [44].

Finally, data analysis represents the bottleneck of intravital imaging. Indeed, it is not an easy task to transform the acquired colorful images and movies in reliable and robust quantitative measurements because of the laser artifacts and animal drifts. However, the improvement of tools for data analysis and, in particular, the ML-based software have been crucial to assist the post-processing of data in a semi-automatic manner. This has not only improved the imaging correction process, but also allowed to increase the sample size, overcoming the efforts deriving from the manual analysis.

In conclusion, we are living in exciting times for in vivo imaging in health and diseases, since 2PM has revealed itself as a powerful tool for improving the knowledge of the kidney physiology in comparison to previous microscopy techniques. Future technical implementations will possibly overcome the existing limitations of 2PM, facilitating the acquisition of real-time high-resolution images and 3D movies in living cells even in different tissues and organs.

References

1. Parslow, A.C.; Clayton, A.H.A.; Lock, P.; Scott, A.M. Confocal Microscopy Reveals Cell Surface Receptor Aggregation Through Image Correlation Spectroscopy. *J. Vis. Exp.* **2018**, *138*, e57164. [CrossRef] [PubMed]
2. Chidambaram, J.D.; Prajna, N.V.; Palepu, S.; Lanjewar, S.; Shah, M.; Elakkiya, S.; Lalitha, P.; Macleod, D.; Burton, M.J. Cellular morphological changes detected by laser scanning in vivo confocal microscopy associated with clinical outcome in fungal keratitis. *Sci. Rep.* **2019**, *9*, 8334. [CrossRef] [PubMed]
3. Costanzo, M.; Caterino, M.; Cevenini, A.; Jung, V.; Chhuon, C.; Lipecka, J.; Fedele, R.; Guerrera, I.C.; Ruoppolo, M. Proteomics Reveals that Methylmalonyl-CoA Mutase Modulates Cell Architecture and Increases Susceptibility to Stress. *Int. J. Mol. Sci.* **2020**, *21*, 4998. [CrossRef] [PubMed]
4. Costanzo, M.; Fiocchetti, M.; Ascenzi, P.; Marino, M.; Caterino, M.; Ruoppolo, M. Proteomic and Bioinformatic Investigation of Altered Pathways in Neuroglobin-Deficient Breast Cancer Cells. *Molecules* **2021**, *26*, 2397. [CrossRef]
5. Costanzo, M.; Caterino, M.; Cevenini, A.; Jung, V.; Chhuon, C.; Lipecka, J.; Fedele, R.; Guerrera, I.C.; Ruoppolo, M. Dataset of a comparative proteomics experiment in a methylmalonyl-CoA mutase knockout HEK 293 cell model. *Data Br.* **2020**, *33*, 106453. [CrossRef]
6. Gonzalez Melo, M.; Remacle, N.; Cudré-Cung, H.-P.; Roux, C.; Poms, M.; Cudalbu, C.; Barroso, M.; Gersting, S.W.; Feichtinger, R.G.; Mayr, J.A.; et al. The first knock-in rat model for glutaric aciduria type I allows further insights into pathophysiology in brain and periphery. *Mol. Genet. Metab.* **2021**, *133*, 157–181. [CrossRef]
7. Pygall, S.R.; Whetstone, J.; Timmins, P.; Melia, C.D. Pharmaceutical applications of confocal laser scanning microscopy: The physical characterisation of pharmaceutical systems. *Adv. Drug Deliv. Rev.* **2007**, *59*, 1434–1452. [CrossRef]

8. Prosperi, F.; Suzumoto, Y.; Marzuillo, P.; Costanzo, V.; Jelen, S.; Iervolino, A.; Guarino, S.; La Manna, A.; Miraglia Del Giudice, E.; Perna, A.F.; et al. Characterization of five novel vasopressin V2 receptor mutants causing nephrogenic diabetes insipidus reveals a role of tolvaptan for M272R-V2R mutation. *Sci. Rep.* **2020**, *10*, 16383. [CrossRef]
9. Rigby, P.J.; Goldie, R.G. Confocal microscopy in biomedical research. *Croat. Med. J.* **1999**, *40*, 346–352.
10. Kitamura, A. Pinhole Closure Improves Spatial Resolution in Confocal Scanning Microscopy. In *Live Cell Imaging*; Humana: New York, NY, USA, 2021; pp. 385–389.
11. Ghosh, S.; Nandi, S.; Ghosh, C.; Bhattacharyya, K. Fluorescence Dynamics in the Endoplasmic Reticulum of a Live Cell: Time-Resolved Confocal Microscopy. *ChemPhysChem* **2016**, *17*, 2818–2823. [CrossRef]
12. Ilyin, S.E.; Flynn, M.C.; Plata-Salamán, C.R. Fiber-optic monitoring coupled with confocal microscopy for imaging gene expression in vitro and in vivo. *J. Neurosci. Methods* **2001**, *108*, 91–96. [CrossRef]
13. Pike, J.A.; Styles, I.B.; Rappoport, J.Z.; Heath, J.K. Quantifying receptor trafficking and colocalization with confocal microscopy. *Methods* **2017**, *115*, 42–54. [CrossRef] [PubMed]
14. Peti-Peterdi, J.; Toma, I.; Sipos, A.; Vargas, S.L. Multiphoton Imaging of Renal Regulatory Mechanisms. *Physiology* **2009**, *24*, 88–96. [CrossRef]
15. Helmchen, F.; Denk, W. Deep tissue two-photon microscopy. *Nat. Methods* **2005**, *2*, 932–940. [CrossRef]
16. Hall, A.M.; Molitoris, B.A. Dynamic Multiphoton Microscopy: Focusing Light on Acute Kidney Injury. *Physiology* **2014**, *29*, 334–342. [CrossRef]
17. Benninger, R.K.P.; Piston, D.W. Two-Photon Excitation Microscopy for the Study of Living Cells and Tissues. *Curr. Protoc. Cell Biol.* **2013**, *59*, 4–11. [CrossRef] [PubMed]
18. Göppert-Mayer, M. Über Elementarakte mit zwei Quantensprüngen. *Ann. Phys.* **1931**, *401*, 273–294. [CrossRef]
19. Kaiser, W.; Garrett, C.G.B. Two-Photon Excitation in Two-Photon Excitation in CaF2: Eu2+. *Phys. Rev. Lett.* **1961**, *7*, 229–231. [CrossRef]
20. Sezgin, E. Super-resolution optical microscopy for studying membrane structure and dynamics. *J. Phys. Condens. Matter* **2017**, *29*, 273001. [CrossRef]
21. Gu, M.; Sheppard, C.J.R. Comparison of three-dimensional imaging properties between two-photon and single-photon fluorescence microscopy. *J. Microsc.* **1995**, *177*, 128–137. [CrossRef]
22. Wilson, T. Resolution and optical sectioning in the confocal microscope. *J. Microsc.* **2011**, *244*, 113–121. [CrossRef]
23. Sankaran, J.; Balasubramanian, H.; Tang, W.H.; Ng, X.W.; Röllin, A.; Wohland, T. Simultaneous spatiotemporal super-resolution and multi-parametric fluorescence microscopy. *Nat. Commun.* **2021**, *12*, 1748. [CrossRef] [PubMed]
24. Mondal, P.P. Temporal resolution in fluorescence imaging. *Front. Mol. Biosci.* **2014**, *1*, 11. [CrossRef]
25. Yang, Z.; Samanta, S.; Yan, W.; Yu, B.; Qu, J. Super-resolution Microscopy for Biological Imaging. In *Optical Imaging in Human Disease and Biological Research*; Springer: Cham, Switzerland, 2021; pp. 23–43.
26. Fahrbach, F.O.; Gurchenkov, V.; Alessandri, K.; Nassoy, P.; Rohrbach, A. Light-sheet microscopy in thick media using scanned Bessel beams and two-photon fluorescence excitation. *Opt. Express* **2013**, *21*, 13824. [CrossRef]
27. Schermelleh, L.; Ferrand, A.; Huser, T.; Eggeling, C.; Sauer, M.; Biehlmaier, O.; Drummen, G.P.C. Super-resolution microscopy demystified. *Nat. Cell Biol.* **2019**, *21*, 72–84. [CrossRef]
28. Urban, B.E.; Yi, J.; Chen, S.; Dong, B.; Zhu, Y.; DeVries, S.H.; Backman, V.; Zhang, H.F. Super-resolution two-photon microscopy via scanning patterned illumination. *Phys. Rev. E* **2015**, *91*, 042703. [CrossRef] [PubMed]
29. Meng, G.; Liang, Y.; Sarsfield, S.; Jiang, W.; Lu, R.; Dudman, J.T.; Aponte, Y.; Ji, N. High-throughput synapse-resolving two-photon fluorescence microendoscopy for deep-brain volumetric imaging in vivo. *Elife* **2019**, *8*, e40805. [CrossRef] [PubMed]
30. Miller, D.R.; Medina, F.A.; Hassan, A.; Perillo, E.P.; Hagan, K.; Shams Kazmi, S.M.; Dunn, A.K. In vivo multiphoton microscopy beyond 1 mm in the brain. In *Optics in the Life Sciences Congress*; OSA: Washington, DC, USA, 2017; p. BrM4B.5.
31. Molitoris, B.A.; Sandoval, R.M. Intravital multiphoton microscopy of dynamic renal processes. *Am. J. Physiol. Physiol.* **2005**, *288*, F1084–F1089. [CrossRef]
32. Zipfel, W.R.; Williams, R.M.; Webb, W.W. Nonlinear magic: Multiphoton microscopy in the biosciences. *Nat. Biotechnol.* **2003**, *21*, 1369–1377. [CrossRef]
33. Svoboda, K.; Yasuda, R. Principles of Two-Photon Excitation Microscopy and Its Applications to Neuroscience. *Neuron* **2006**, *50*, 823–839. [CrossRef]
34. Caterino, M.; Ruoppolo, M.; Costanzo, M.; Albano, L.; Crisci, D.; Sotgiu, G.; Saderi, L.; Montella, A.; Franconi, F.; Campesi, I. Sex Affects Human Premature Neonates' Blood Metabolome According to Gestational Age, Parenteral Nutrition, and Caffeine Treatment. *Metabolites* **2021**, *11*, 158. [CrossRef] [PubMed]
35. Caterino, M.; Ruoppolo, M.; Villani, G.R.D.; Marchese, E.; Costanzo, M.; Sotgiu, G.; Dore, S.; Franconi, F.; Campesi, I. Influence of Sex on Urinary Organic Acids: A Cross-Sectional Study in Children. *Int. J. Mol. Sci.* **2020**, *21*, 582. [CrossRef] [PubMed]
36. Costanzo, M.; Caterino, M.; Fedele, R.; Cevenini, A.; Pontillo, M.; Barra, L.; Ruoppolo, M. COVIDomics: The Proteomic and Metabolomic Signatures of COVID-19. *Int. J. Mol. Sci.* **2022**, *23*, 2414. [CrossRef] [PubMed]
37. Hall, A.M.; Unwin, R.J.; Parker, N.; Duchen, M.R. Multiphoton Imaging Reveals Differences in Mitochondrial Function between Nephron Segments. *J. Am. Soc. Nephrol.* **2009**, *20*, 1293–1302. [CrossRef]
38. Sandoval, R.M.; Molitoris, B.A. Intravital multiphoton microscopy as a tool for studying renal physiology and pathophysiology. *Methods* **2017**, *128*, 20–32. [CrossRef] [PubMed]

39. Bugarski, M.; Martins, J.R.; Haenni, D.; Hall, A.M. Multiphoton imaging reveals axial differences in metabolic autofluorescence signals along the kidney proximal tubule. *Am. J. Physiol. Physiol.* **2018**, *315*, F1613–F1625. [CrossRef]

40. Caterino, M.; Costanzo, M.; Fedele, R.; Cevenini, A.; Gelzo, M.; Di Minno, A.; Andolfo, I.; Capasso, M.; Russo, R.; Annunziata, A.; et al. The Serum Metabolome of Moderate and Severe COVID-19 Patients Reflects Possible Liver Alterations Involving Carbon and Nitrogen Metabolism. *Int. J. Mol. Sci.* **2021**, *22*, 9548. [CrossRef]

41. Shanley, P.F.; Brezis, M.; Spokes, K.; Silva, P.; Epstein, F.H.; Rosen, S. Differential Responsiveness of Proximal Tubule Segments to Metabolic Inhibitors in the Isolated Perfused Rat Kidney. *Am. J. Kidney Dis.* **1986**, *7*, 76–83. [CrossRef]

42. Hall, A.M.; Rhodes, G.J.; Sandoval, R.M.; Corridon, P.R.; Molitoris, B.A. In vivo multiphoton imaging of mitochondrial structure and function during acute kidney injury. *Kidney Int.* **2013**, *83*, 72–83. [CrossRef]

43. Manganelli, V.; Salvatori, I.; Costanzo, M.; Capozzi, A.; Caissutti, D.; Caterino, M.; Valle, C.; Ferri, A.; Sorice, M.; Ruoppolo, M.; et al. Overexpression of Neuroglobin Promotes Energy Metabolism and Autophagy Induction in Human Neuroblastoma SH-SY5Y Cells. *Cells* **2021**, *10*, 3394. [CrossRef]

44. Hato, T.; Winfree, S.; Dagher, P.C. Intravital imaging of the kidney. *Methods* **2017**, *128*, 33–39. [CrossRef]

45. Zipfel, W.R.; Williams, R.M.; Christie, R.; Nikitin, A.Y.; Hyman, B.T.; Webb, W.W. Live tissue intrinsic emission microscopy using multiphoton-excited native fluorescence and second harmonic generation. *Proc. Natl. Acad. Sci. USA* **2003**, *100*, 7075–7080. [CrossRef]

46. Reeve, J.E.; Anderson, H.L.; Clays, K. Dyes for biological second harmonic generation imaging. *Phys. Chem. Chem. Phys.* **2010**, *12*, 13484. [CrossRef]

47. Small, D.M.; Sanchez, W.Y.; Gobe, G.C. Intravital Multiphoton Imaging of the Kidney: Tubular Structure and Metabolism. In *Kidney Research*; Humana Press: New York, NY, USA, 2016; pp. 155–172.

48. Strupler, M.; Hernest, M.; Fligny, C.; Martin, J.-L.; Tharaux, P.-L.; Schanne-Klein, M.-C. Second harmonic microscopy to quantify renal interstitial fibrosis and arterial remodeling. *J. Biomed. Opt.* **2008**, *13*, 054041. [CrossRef]

49. Nucciotti, V.; Stringari, C.; Sacconi, L.; Vanzi, F.; Fusi, L.; Linari, M.; Piazzesi, G.; Lombardi, V.; Pavone, F.S. Probing myosin structural conformation in vivo by second-harmonic generation microscopy. *Proc. Natl. Acad. Sci. USA* **2010**, *107*, 7763–7768. [CrossRef]

50. Yu, C.-H.; Langowitz, N.; Wu, H.-Y.; Farhadifar, R.; Brugues, J.; Yoo, T.Y.; Needleman, D. Measuring Microtubule Polarity in Spindles with Second-Harmonic Generation. *Biophys. J.* **2014**, *106*, 1578–1587. [CrossRef]

51. Petrillo, F.; Iervolino, A.; Angrisano, T.; Jelen, S.; Costanzo, V.; D'Acierno, M.; Cheng, L.; Wu, Q.; Guerriero, I.; Mazzarella, M.C.; et al. Dysregulation of Principal Cell miRNAs Facilitates Epigenetic Regulation of AQP2 and Results in Nephrogenic Diabetes Insipidus. *J. Am. Soc. Nephrol.* **2021**, *32*, 1339–1354. [CrossRef]

52. Ranjit, S.; Dobrinskikh, E.; Montford, J.; Dvornikov, A.; Lehman, A.; Orlicky, D.J.; Nemenoff, R.; Gratton, E.; Levi, M.; Furgeson, S. Label-free fluorescence lifetime and second harmonic generation imaging microscopy improves quantification of experimental renal fibrosis. *Kidney Int.* **2016**, *90*, 1123–1128. [CrossRef]

53. Perry, S.W.; Burke, R.M.; Brown, E.B. Two-Photon and Second Harmonic Microscopy in Clinical and Translational Cancer Research. *Ann. Biomed. Eng.* **2012**, *40*, 277–291. [CrossRef]

54. Caterino, M.; Zacchia, M.; Costanzo, M.; Bruno, G.; Arcaniolo, D.; Trepiccione, F.; Siciliano, R.A.; Mazzeo, M.F.; Ruoppolo, M.; Capasso, G. Urine Proteomics Revealed a Significant Correlation Between Urine-Fibronectin Abundance and Estimated-GFR Decline in Patients with Bardet-Biedl Syndrome. *Kidney Blood Press. Res.* **2018**, *43*, 389–405. [CrossRef]

55. Gonzalez Melo, M.; Fontana, A.; Viertl, D.; Allenbach, G.; Prior, J.O.; Rotman, S.; Feichtinger, R.G.; Mayr, J.A.; Costanzo, M.; Caterino, M.; et al. A knock-in rat model unravels acute and chronic renal toxicity in glutaric aciduria type I. *Mol. Genet. Metab.* **2021**, *134*, 287–300. [CrossRef] [PubMed]

56. Denic, A.; Mathew, J.; Lerman, L.O.; Lieske, J.C.; Larson, J.J.; Alexander, M.P.; Poggio, E.; Glassock, R.J.; Rule, A.D. Single-Nephron Glomerular Filtration Rate in Healthy Adults. *N. Engl. J. Med.* **2017**, *376*, 2349–2357. [CrossRef]

57. Vallon, V. Micropuncturing the nephron. *Pflügers Arch. Eur. J. Physiol.* **2009**, *458*, 189–201. [CrossRef]

58. Kang, J.J.; Toma, I.; Sipos, A.; McCulloch, F.; Peti-Peterdi, J. Quantitative imaging of basic functions in renal (patho)physiology. *Am. J. Physiol. Physiol.* **2006**, *291*, F495–F502. [CrossRef] [PubMed]

59. Costanzo, V.; D'Apolito, L.; Sardella, D.; Iervolino, A.; La Manna, G.; Capasso, G.; Frische, S.; Trepiccione, F. Single nephron glomerular filtration rate measured by linescan multiphoton microscopy compared to conventional micropuncture. *Pflügers Arch. Eur. J. Physiol.* **2022**. online ahead of print. [CrossRef]

60. Ferrell, N.; Sandoval, R.M.; Bian, A.; Campos-Bilderback, S.B.; Molitoris, B.A.; Fissell, W.H. Shear stress is normalized in glomerular capillaries following 5/6 nephrectomy. *Am. J. Physiol. Physiol.* **2015**, *308*, F588–F593. [CrossRef]

61. Ciarimboli, G.; Schlatter, E. Regulation of organic cation transport. *Pflügers Arch. Eur. J. Physiol.* **2005**, *449*, 423–441. [CrossRef]

62. Motohashi, H.; Inui, K. Organic Cation Transporter OCTs (SLC22) and MATEs (SLC47) in the Human Kidney. *AAPS J.* **2013**, *15*, 581–588. [CrossRef] [PubMed]

63. Cohen, G.; Glorieux, G.; Thornalley, P.; Schepers, E.; Meert, N.; Jankowski, J.; Jankowski, V.; Argiles, A.; Anderstam, B.; Brunet, P.; et al. Review on uraemic toxins III: Recommendations for handling uraemic retention solutes in vitro towards a standardized approach for research on uraemia. *Nephrol. Dial. Transplant.* **2007**, *22*, 3381–3390. [CrossRef] [PubMed]

64. Hörbelt, M.; Wotzlaw, C.; Sutton, T.A.; Molitoris, B.A.; Philipp, T.; Kribben, A.; Fandrey, J.; Pietruck, F. Organic cation transport in the rat kidney in vivo visualized by time-resolved two-photon microscopy. *Kidney Int.* **2007**, *72*, 422–429. [CrossRef]

65. Engbjerg, J.S.; Costanzo, V.; Sardella, D.; Bordoni, L.; Jakobsen, S.; D'Apolito, L.; Frøkiær, J.; Trepiccione, F.; Capasso, G.; Frische, S. The Probe for Renal Organic Cation Secretion (4-Dimethylaminostyryl)-N-Methylpyridinium (ASP+)) Shows Amplified Fluorescence by Binding to Albumin and Is Accumulated In Vivo. *Mol. Imaging* **2022**, *2022*, 7908357. [CrossRef]
66. Meyer-Schwesinger, C. The Role of Renal Progenitors in Renal Regeneration. *Nephron* **2016**, *132*, 101–109. [CrossRef]
67. Schiessl, I.M.; Grill, A.; Fremter, K.; Steppan, D.; Hellmuth, M.-K.; Castrop, H. Renal Interstitial Platelet-Derived Growth Factor Receptor- β Cells Support Proximal Tubular Regeneration. *J. Am. Soc. Nephrol.* **2018**, *29*, 1383–1396. [CrossRef]
68. Zhang, K.; Chen, S.; Sun, H.; Wang, L.; Li, H.; Zhao, J.; Zhang, C.; Li, N.; Guo, Z.; Han, Z.; et al. In vivo two-photon microscopy reveals the contribution of Sox9+ cell to kidney regeneration in a mouse model with extracellular vesicle treatment. *J. Biol. Chem.* **2020**, *295*, 12203–12213. [CrossRef]
69. Rhodes, G.J. Surgical preparation of rats and mice for intravital microscopic imaging of abdominal organs. *Methods* **2017**, *128*, 129–138. [CrossRef]
70. Dunn, K.W.; Sutton, T.A.; Sandoval, R.M. Live-Animal Imaging of Renal Function by Multiphoton Microscopy. *Curr. Protoc. Cytom.* **2018**, *83*, 12–19. [CrossRef]
71. Soulet, D.; Lamontagne-Proulx, J.; Aubé, B.; Davalos, D. Multiphoton intravital microscopy in small animals: Motion artefact challenges and technical solutions. *J. Microsc.* **2020**, *278*, 3–17. [CrossRef]
72. Flotho, P.; Nomura, S.; Kuhn, B.; Strauss, D.J. Software for Non-Parametric Image Registration of 2-Photon Imaging Data. *J. Biophotonics* **2022**, e202100330, online ahead of print. [CrossRef]
73. Ritsma, L.; Steller, E.J.A.; Ellenbroek, S.I.J.; Kranenburg, O.; Borel Rinkes, I.H.M.; van Rheenen, J. Surgical implantation of an abdominal imaging window for intravital microscopy. *Nat. Protoc.* **2013**, *8*, 583–594. [CrossRef]
74. Bölke, T.; Krapf, L.; Orzekowsky-Schroeder, R.; Vossmeyer, T.; Dimitrijevic, J.; Weller, H.; Schüth, A.; Klinger, A.; Hüttmann, G.; Gebert, A. Data-adaptive image-denoising for detecting and quantifying nanoparticle entry in mucosal tissues through intravital 2-photon microscopy. *Beilstein J. Nanotechnol.* **2014**, *5*, 2016–2025. [CrossRef]
75. Xiao, S.; Mertz, J. Contrast improvement in two-photon microscopy with instantaneous differential aberration imaging. *Biomed. Opt. Express* **2019**, *10*, 2467. [CrossRef] [PubMed]
76. Kan, A. Machine learning applications in cell image analysis. *Immunol. Cell Biol.* **2017**, *95*, 525–530. [CrossRef] [PubMed]
77. Mougeot, G.; Dubos, T.; Chausse, F.; Péry, E.; Graumann, K.; Tatout, C.; Evans, D.E.; Desset, S. Deep learning—Promises for 3D nuclear imaging: A guide for biologists. *J. Cell Sci.* **2022**, *135*, jcs258986. [CrossRef]
78. Wang, S.; Zhou, Y.; Qin, X.; Nair, S.; Huang, X.; Liu, Y. Label-free detection of rare circulating tumor cells by image analysis and machine learning. *Sci. Rep.* **2020**, *10*, 12226. [CrossRef] [PubMed]
79. Ruini, C.; Schlingmann, S.; Jonke, Ž.; Avci, P.; Padrón-Laso, V.; Neumeier, F.; Koveshazi, I.; Ikeliani, I.U.; Patzer, K.; Kunrad, E.; et al. Machine Learning Based Prediction of Squamous Cell Carcinoma in Ex Vivo Confocal Laser Scanning Microscopy. *Cancers* **2021**, *13*, 5522. [CrossRef] [PubMed]
80. Kromp, F.; Bozsaky, E.; Rifatbegovic, F.; Fischer, L.; Ambros, M.; Berneder, M.; Weiss, T.; Lazic, D.; Dörr, W.; Hanbury, A.; et al. An annotated fluorescence image dataset for training nuclear segmentation methods. *Sci. Data* **2020**, *7*, 262. [CrossRef]
81. Berg, S.; Kutra, D.; Kroeger, T.; Straehle, C.N.; Kausler, B.X.; Haubold, C.; Schiegg, M.; Ales, J.; Beier, T.; Rudy, M.; et al. ilastik: Interactive machine learning for (bio)image analysis. *Nat. Methods* **2019**, *16*, 1226–1232. [CrossRef] [PubMed]
82. Martins, J.R.; Haenni, D.; Bugarski, M.; Polesel, M.; Schuh, C.; Hall, A.M. Intravital kidney microscopy: Entering a new era. *Kidney Int.* **2021**, *100*, 527–535. [CrossRef]
83. Dunn, K.W.; Sandoval, R.M.; Kelly, K.J.; Dagher, P.C.; Tanner, G.A.; Atkinson, S.J.; Bacallao, R.L.; Molitoris, B.A. Functional studies of the kidney of living animals using multicolor two-photon microscopy. *Am. J. Physiol. Physiol.* **2002**, *283*, C905–C916. [CrossRef]
84. Hackl, M.J.; Burford, J.L.; Villanueva, K.; Lam, L.; Suszták, K.; Schermer, B.; Benzing, T.; Peti-Peterdi, J. Tracking the fate of glomerular epithelial cells in vivo using serial multiphoton imaging in new mouse models with fluorescent lineage tags. *Nat. Med.* **2013**, *19*, 1661–1666. [CrossRef]
85. Rovira-Halbach, G.; Alt, J.M.; Brunkhorst, R.; Frei, U.; Kühn, K.; Stolte, H. Single nephron hyperfiltration and proteinuria in a newly selected rat strain with superficial glomeruli. *Ren. Physiol.* **1986**, *9*, 317–325. [CrossRef]
86. Saritas, T.; Puelles, V.G.; Su, X.-T.; Ellison, D.H.; Kramann, R. Optical Clearing and Imaging of Immunolabeled Kidney Tissue. *J. Vis. Exp.* **2019**, *149*, e60002. [CrossRef]
87. Lin, M.-H.; Chen, J.-C.; Tian, X.; Lee, C.-M.; Yu, I.-S.; Lo, Y.-F.; Uchida, S.; Huang, C.-L.; Chen, B.-C.; Cheng, C.-J. Impairment in renal medulla development underlies salt wasting in Clc-k2 channel deficiency. *JCI Insight* **2021**, *6*, e151039. [CrossRef]